JOURNAL OF MATERIALS SCIENCE 26 (1991) 6325–6330

High-resolution electron microscopy of the twinning and intergrowth in $Ca_4Al_6SO_{16}$ and $Ca_3SrAl_6SO_{16}$

Y. G. WANG, H. Q. YE, K. H. KUO, X. J. FENG*, S. Z. LONG*, G. L. LAO*
Laboratory of Atomic Imaging of Solids, Institute of Metal Research, Academia Sinica, Shenyang 110015, People's Republic of China

The microstructures of unhydrated calcium aluminosulphate $Ca_4Al_6SO_{16}$ and $Ca_3SrAl_6SO_{16}$ have been studied by high-resolution electron microscopy (HREM). The results showed that twinning and twinned slabs could be introduced taking the [1 1 2] direction as the twin axis so that it seems to be coincident with the law of twinning formed in body-centred cubic structures. A previously reported superlattice with a repeat period twice that of the fundamental structure along the ⟨1 1 0⟩ direction has also been found in both matrix and twin variants. The close intergrowth of $Ca_3SrAl_6SO_{16}$ and another phase, possibly $Sr_3Al_2O_6$ existing as an inclusion between these two twin variants, was determined and clearly revealed by electron diffraction and HREM images. The coherent interphase boundaries and orientation relationship between them can also be deduced.

1. Introduction

The cement of calcium aluminosulphate $Ca_4Al_6SO_{16}$ (usually abbreviated as C_4A_3S) was first reported by Ragozina in 1957 [1] and its structure was analysed by Halsted and Moore [2] using X-ray powder diffraction. Their results showed that C_4A_3S has an ultramarine-like structure: the continuous framework constructed by linked alumina-oxygen tetrahedra and its Bravias lattice was satisfied with a body-centred cubic lattice with a cell parameter of approximately 0.9 nm. The space group was suggested to be $I\bar{4}3m$. Recently Feng *et al.* [3] have confirmed these conclusions, and the positions of atoms in C_4A_3S have also been examined: the result is shown in Fig. 1a, in which the two sets of 8c position are demonstrated. This suggests that the calcium cations could oscillate slightly near their equilibrium positions or move from place to place along the channels of this framework, built by alumina-oxygen tetrahedra, in the direction of body diagonals of the unit cell. This is in agreement with the conclusion of Jaeger [4] in his study of ultramarine that certain cations are in an errant state within such a framework. $Ca_3SrAl_6SO_{16}$ may also be considered to be a cement compound with an ultramarine-like structure because it has the same arrangement of atoms as C_4A_3S [5].

Early studies of X-ray and electron diffraction have shown superlattice reflections along the ⟨1 1 0⟩ direction, implying the existence of superstructures in these cement clinkers. A detailed study utilizing high-resolution electron microscopy (HREM) has already been carried out by us [6]; the result showed these superstructures to have a very close relationship with the ordering distribution of calcium cations in crystals.

In order to interpret the experimental images unambiguously, image simulation has been carried out using the dynamic multislice program written by Ishizuka [7]. The optimum defocus value of -65.0 nm, corresponding to the first broad band in the transfer function for $C_s = 1.2$ mm at accelerating voltage of 200 kV, was used. By calculating the variation in the statistically independent fluctuations in accelerating voltage and objective current, the half-width of a Gaussian spread of defocus is 7.0 nm at the experimental gun bias. The semi-angle of convergence of the incident beam, $\theta_c/\lambda = 0.30$ rad nm^{-1}, can be estimated from a focused condenser aperture diffraction pattern. The size limited by the objective aperture, $(\sin\theta)/\lambda = 0.35$ nm^{-1}, can be measured from a double-exposed diffraction pattern. A through-focus series of the lattice images was found to be in good agreement with simulated images. Fig. 1b and c show a pair of images at Scherzer defocus for a thickness of 4.5 nm, where each bright dot in the images corresponds to a column of sulphur atoms in the projected structure model (Fig. 1a). Such a good correspondence suggests that the structural image taken at the Scherzer defocus condition could be used to interpret the structural irregularity in crystal of C_4A_3S occurring within local areas directly.

2. Experimental procedure

The specimen under investigation was prepared by mixing the raw materials of CaO, SrO, Al_2O_3 and $CaSO_4$ according to the nominal compositions of $3CaO:3Al_2O_3:CaSO_4$ and $2CaO:SrO:3Al_2O_3:CaSO_4$, respectively. The uniform powder mixture was pressed

* Also at *Wuhan University of Technology, Luoshi Road 14, Wuhan 470030, People's Republic of China*

0022–2461/91 $03.00 + .12

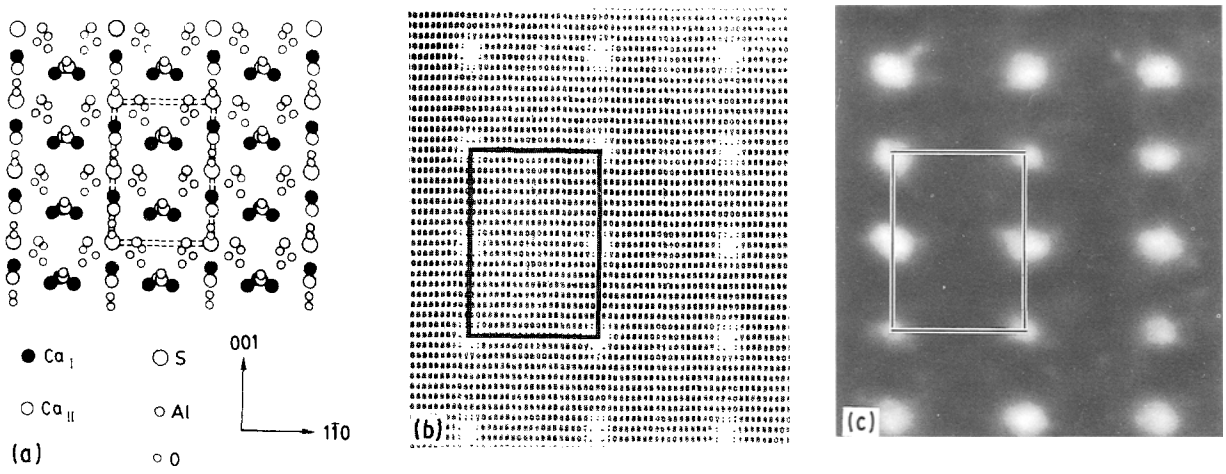

Figure 1 (a) Schematic projection of C_4A_3S along the [1 1 0] direction and (b) a simulated image calculated at a thickness of 4.5 nm and the Scherzer defocus value ($\Delta f = -65.0$ nm) showing a good correspondence of bright dots and columns of sulphur atoms in the structure. (c) [1 1 0] high-resolution lattice image taken at the Scherzer defocus condition.

in a cylindrical mould at 150 MPa, and the resulting compact pieces were sintered in the platinum container of a furnace; the details of the experimental procedure are described in our previous paper [6]. Samples suitable for HREM observations were made by carefully grinding some of these clinkers into thin pieces in an agate mortar, and suspended in absolute alcohol. A drop of this suspension was placed on copper grids coated with holed carbon film. The samples were examined with a JEOL-200CX electron microscope equipped with a top-entry goniometer stage and an ultra-high resolution pole piece ($C_s = 1.2$ mm) having an interpretable resolution of 0.25 nm. Various crystals with $\langle 1\,1\,0 \rangle$ orientations were intentionally chosen so that the images always included $\{1\,1\,2\}$ planes or $\langle 1\,1\,2 \rangle$ directions, in order to make it is easy to identify these twinnings if they were indeed present. All high-resolution images were, as far as possible, taken under symmetrical incidence conditions in order to interpret them directly according to the above results of image simulation. Low beam current density was used for the observations because these cement compounds are all sensitive to electron-beam damage irradiation; as usual an image intensifier was also used in order to solve this problem.

3. Results and discussion

3.1. Twinning in the C_4A_3S matrix

Because C_4A_3S has a body-centred cubic lattice, the twinning (if present in this compound) can be predicted to be constructed in mirror reflections taking $\{1\,1\,2\}$ planes as the twin interfaces, or 180° rotations with $\langle 1\,1\,2 \rangle$ directions as the twin axes, according to studies on the law of twinning formed in crystals with such Bravias lattices [8], although there have not been any reports about them in this cement yet.

Recently, we have luckily found a composited electron diffraction pattern from bicrystals of the C_4A_3S matrix as shown in Fig. 2, obtained by orienting the crystal to have its $[\bar{1}\,1\,0]$ direction parallel to the incident beam, in which the two sets of reflection could be divided easily and outlined in white lines. The

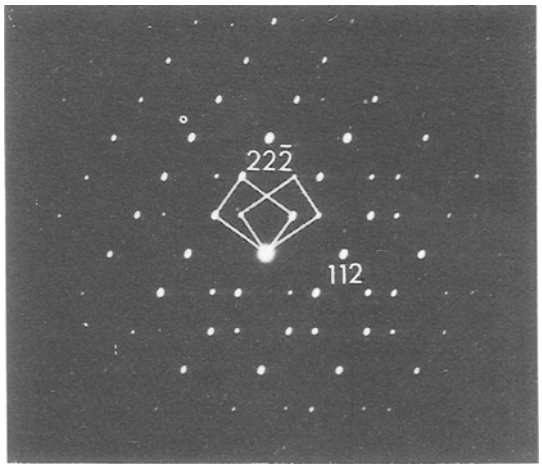

Figure 2 An electron diffraction pattern obtained with the incident beam parallel with the $[\bar{1}\,1\,0]$ direction showing the twinning of the C_4A_3S matrix.

characteristic feature of these patterns is that the reflection spots shift along the [1 1 2]* direction mutually with a magnitude of 1/3 of the distance between the two main spots in the same direction, so that the repeat period is three rows, i.e. there will be one row of spots in every three, ranking horizontally and located in coincident sites. The characteristic arrangement of spots in Fig. 2 makes it clear that the bicrystals of C_4A_3S are actually in twin-related orientations. The indices of the diffraction spots due to the twin, in terms of the matrix reciprocal lattice, can be deduced from a formula already given in the literature [9]. After twinning, $h\,k\,l$ becomes $h'\,k'\,l'$ and

$$h' = \bar{h} + (h + k + 2l)/3,\ k' = \bar{k} + (h + k + 2l)/3,\ l' = \bar{l} + 2(h + k + 2l)/3 \quad (1)$$

Therefore the indices of diffraction spots due to the twinning in Fig. 2 can be expressed in terms of matrix spots by Equation 1. The $h'\,k'\,l'$ spots of the twin can be obtained by moving the $h\,k\,l$ spots of the matrix along the [1 1 2]* direction by 1/3 of the value of the [1 1 2]* vector, and for the spots with $h + k + 2l = 3n$, the spots of the twin's $h'\,k'\,l'$ are all integers

and coincide with those of the matrix. Consequently the 1/3 lattice points of the matrix and the twin are coincident in both real and reciprocal spaces, respectively, and thus it is a twinning with $\Sigma = 3$ [10]. However, it is still uncertain whether the twinning constructed in the (1 1 2) mirror reflection or the [1 1 2] 180° rotation can be examined unambiguously in electron diffraction patterns. Fig. 3 is the corresponding high-resolution structural image showing the fine structure of twin-related bicrystals of C_4A_3S and their outlined unit cells. There is a very sharp interface parallel to the (1 1 $\bar{1}$) plane or the [1 1 2] direction (marked by arrows and the letters TB) connecting the two twinned variants. Thus the information revealed in the HREM image (Fig. 3) suggests that the twinning is possibly satisfied with the [1 1 2] 180° rotation case, i.e. taking [1 1 2] as twin axis, and after 180° rotation around this axis the two twin variants will be coincident with each other. This is different from the body-centred cubic close-packed structure; in the latter case, such twinning may be introduced by a simple displacement of atoms on the (1 1 $\bar{1}$) plane. From image simulations, it is known that the bright dot in Fig. 3 corresponds to the column of sulphur atoms in the projected structure (Fig. 1a), and therefore the structure model of such [1 1 2] 180°-rotation twinning could be suggested, as shown in Fig. 4. The twin boundary here may correspond to a non-stoichiometric interface, so that a non-conservative interface is formed, i.e. the framework at the twin interface is greatly distorted and the ratio of cations and ions reduced. As a result an interface related to the deficit of cations or excess of ions may be caused. Therefore it is in fact distinct from the twinnings in body-centred cubic close-packed structures, as for these the twin boundary is stoichiometric and thus a conservative interface is preserved between the two twin-related variants. On the other hand, a possible explanation of the observed microstructure may be that this twinning formed on the initial stage of crystal nucleation during the process of preparation, because the non-stoichiometric interface cannot be introduced by simple displacement of atoms caused by the shear stress crystals with an ultramarine structure. This also means that the twin boundary corresponding to the fluctuation of cations or ions may be a pre-existing linear or planar defect at the beginning of crystal nucleation which was maintained in the process of crystal growth. Thus the formation of this twinning seems to be coincident with the growth mechanism.

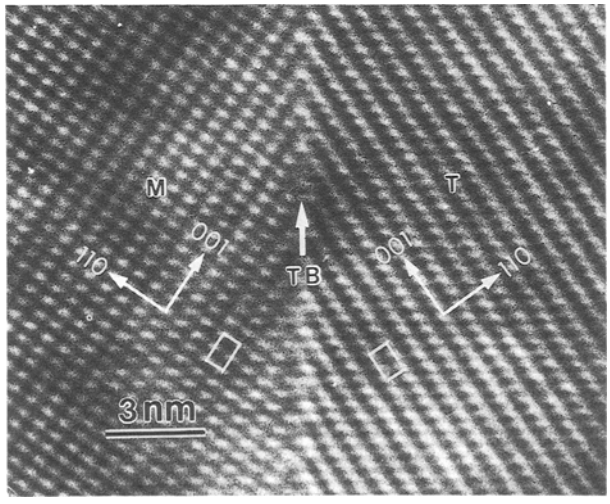

Figure 3 [$\bar{1}$ 1 0] HREM image showing [1 1 2] rotation twinning, the twin boundary (TB) marked by arrows.

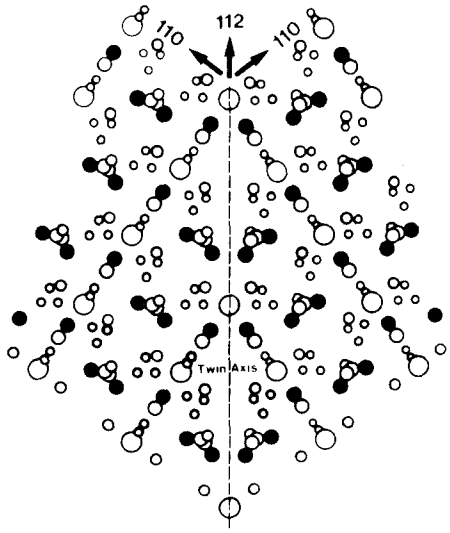

Figure 4 A suggested structure model of the [1 1 2] rotation twinning. The dash line indicates the twin axis, and there is a relative displacement between the two twin variants. Heights of atoms in the projected structure model are omitted for simplicity.

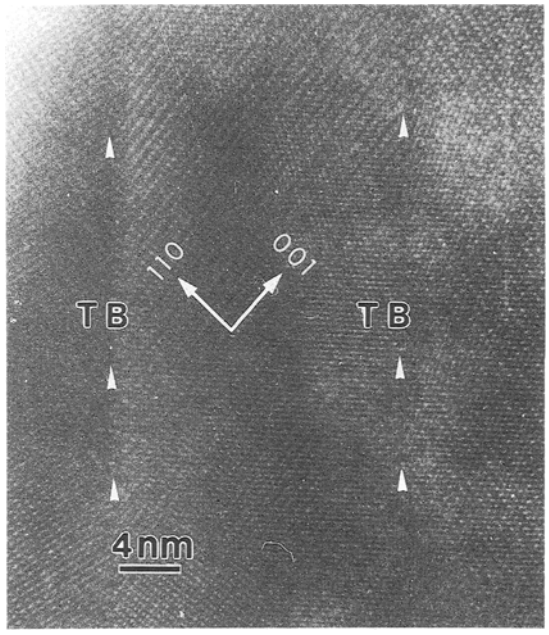

Figure 5 [$\bar{1}$ 1 0] HREM image demonstrating the multiple twinnings in C_4A_3S matrix.

The multiple twinnings are also determined in this cement clinker and demonstrated in Fig. 5, where a twinned slab about 15.0 nm wider is clearly shown. The presence of such multiple twinnings with non-conservative interfaces would also introduce a non-stoichiometric structure in the matrix. For comparison, $Ca_3SrAl_6SO_{16}$ was also examined by HREM and this twin structure has been found.

3.2. Twinning in the superstructure

It is known that the $2*d_{1\,1\,0}$ superstructure frequently presents in the C_4A_3S matrix, and therefore we can predict that it may be produced in the twin variants as well. Fig. 6 is an electron diffraction pattern in the same direction as Fig. 2. This shows two sets of reflections showing the feature of [1 1 2] 180° rotation twinning, and also a superlattice reflection spot appearing mid-way between two main spots of the basic structure along the [1 1 0] direction in one set of the reflection. Therefore the $2*d_{1\,1\,0}$ superstructure was introduced in one twin variant, confirmed by the corresponding high-resolution lattice image (Fig. 7), where at the right variant the repeat period of twice of that of the fundamental unit cell (left) is clearly exhibited. As a result the intergrowth of matrix and superstructure in the twin orientation relationship is formed in addition to the presence of this superstructure in the matrix, as well as the co-existence of various orientation variants of this superstructure already reported [9].

Fig. 8 shows the [$\bar{1}$ 1 0] electron diffraction pattern, illustrating the existence of [1 1 2] 180° rotation twinning in the case of the $2*d_{1\,1\,0}$ superstructure: the satellite spots corresponding to the $2*d_{1\,1\,0}$ superlattices are all present in two sets of reflections. The corresponding high-resolution lattice image is shown in Fig. 9. Within this figure the lattice with double space $d_{1\,1\,0}$ of the matrix can be seen and marked out in both twin variants. The misfit twin interfaces are also illustrated. Therefore the [1 1 2] 180° rotation twinning can be constructed in the $2*d_{1\,1\,0}$ superstructure, and in this case it can be predicted that the twin boundary is also a non-stoichiometric one and the non-conservative interface may be produced equally. On the other hand, this [1 1 2] 180° rotation-related superstructure may be treated as a special kind of orientation variant which is not related by the symmetrical elements in the fundamental structure. Thus the orientation angle of these variants is not limited by these symmetrical operations. This value can be calculated from the diffraction pattern and equals 70.5°, being a new kind of orientation variant in addition to those reported for 90° and 120°. As a result, there will be three kinds of orientation variant in the case of the $2*d_{1\,1\,0}$ superstructure.

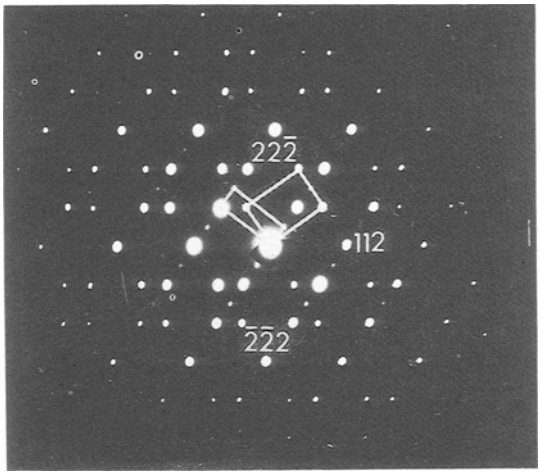

Figure 6 Electron diffraction showing the $2*d_{1\,1\,0}$ superstructure formed in twin variants and unit cells of the reciprocal lattice of both fundamental structure and superstructure.

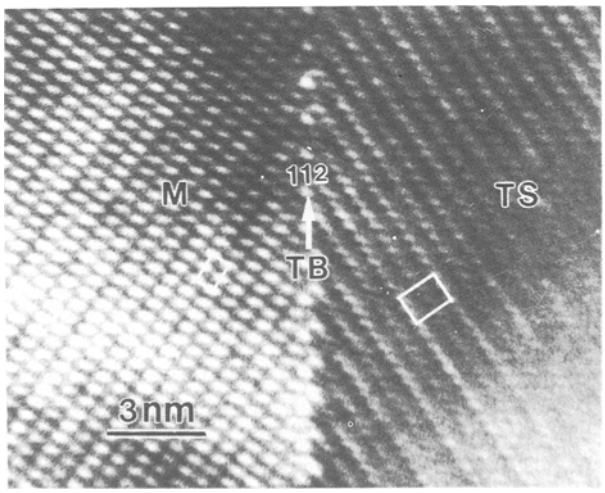

Figure 7 [$\bar{1}$ 1 0] HREM image illustrating the $2*d_{1\,1\,0}$ superstructure introduced inside the twin variant (TS) area.

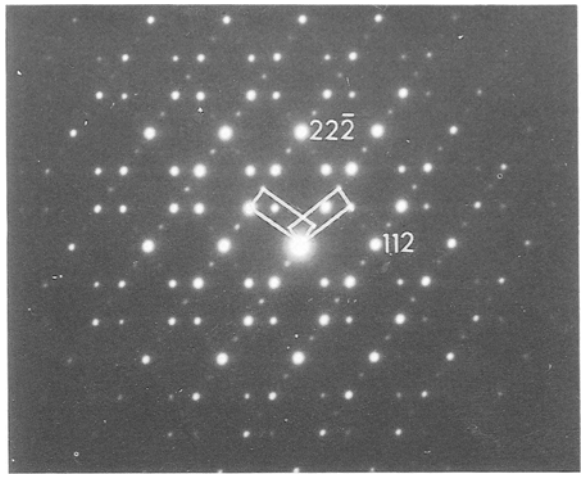

Figure 8 An electron diffraction pattern in the [$\bar{1}$ 1 0] orientation showing the twin-oriented $2*d_{1\,1\,0}$ superstructures.

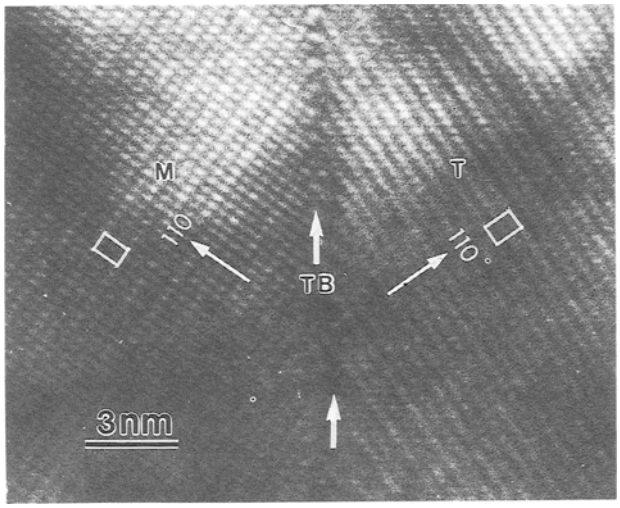

Figure 9 [$\bar{1}$ 1 0] HREM image exhibiting the [1 1 2] 180° rotation twinning in the case of the $2*d_{1\,1\,0}$ superstructure.

3.3. Intergrowth of the superstructures of $Ca_3SrAl_6SO_{16}$ and $Sr_3Al_2O_6$

Although the most abundant phases in this cement compound are the $Ca_3SrAl_6SO_{16}$ matrix and various related superstructures [11], there is also another phase found in co-existence with the $2*d_{1\,1\,0}$ superstructure of $Ca_3SrAl_6SO_{16}$. Fig. 10 is a selected-area electron diffraction pattern with incident beam parallel to the $[\bar{1}\,1\,0]$ direction of $Ca_3SrAl_6SO_{16}$. Besides the two sets of $2*d_{1\,1\,0}$ superlattice reflection related by 180° rotation around the $[1\,1\,2]^*$ axis, there are also some very weak reflection spots appearing along both the $[1\,1\,2]^*$ and $[1\,1\,\bar{1}]^*$ directions, respectively, as indicated by arrows. Since the superstructures along these two directions have already been detected [11], it is difficult to decide whether the ordering of cations or other phases causes these extra spots. However the intergrowth of twinning of the $2*d_{1\,1\,0}$ superstructure and other phases is confirmed by the corresponding high-resolution image (Fig. 11). Here a band-like area with darker contrast exists as an inclusion between the two twin variants, but superstructures other than the $2*d_{1\,1\,0}$ are not found. Parallel intergrowth is definitely shown, and the interface is arranged along the $(1\,1\,\bar{1})$ plane or the $[1\,1\,2]$ twin axis. The multiple intergrowth ledges on $(1\,1\,2)$, as well as step-like interfaces, are also exhibited and marked by arrows. The extra spots will disappear from the electron diffraction pattern obtained by putting the field-selected aperture on either one of the two twin variants in Fig. 11. Therefore the included slab is a different phase. The two spots exactly located at the fractional positions between the two main reflection spots of the $Ca_3SrAl_6SO_{16}$ matrix along those two directions mean that this phase may have a very close relationship with the host in structural aspects or in the lattice parameter. The coherent interphase boundary between these two phases may be assumed to be based on the composited electron diffraction pattern and is confirmed by the corresponding high-resolution image (Fig. 11). The repeat periods of 1.12 and 0.79 nm along the $[1\,1\,2]$ and $[1\,1\,\bar{1}]$ directions are calculated,

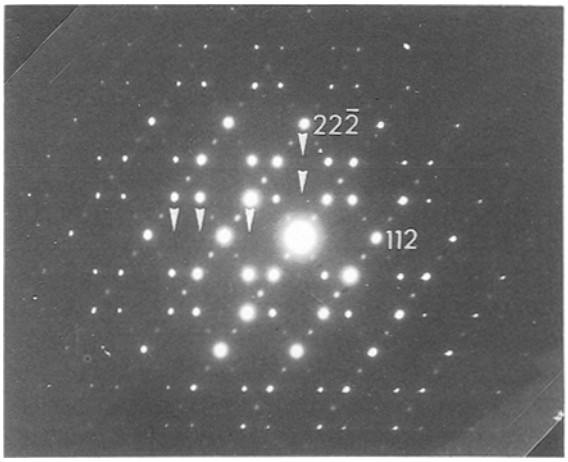

Figure 10 A $[\bar{1}\,1\,0]$ zone electron diffraction pattern of twinned $2*d_{1\,1\,0}$ superstructures, in which two weak spots are indicated by arrows along the $[1\,1\,\bar{1}]^*$ and $[1\,1\,2]^*$ directions, respectively, implying the intergrowth of this superstructure and $Sr_3Al_2O_6$.

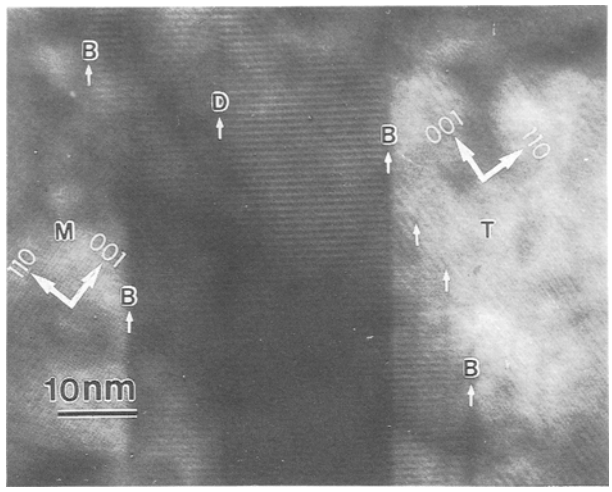

Figure 11 A general view of the parallel intergrowth of twin-related $2*d_{1\,1\,0}$ superstructures and the $Sr_3Al_2O_6$ phase located in the central area as an inclusion. As a result the coherent interfaces parallel with the $(1\,1\,\bar{1})$ plane and multiple intergrowth ledges on $(1\,1\,2)$ at B, as well as the planar defect at D (indicated by arrows) are all introduced.

based on Fig. 10, to correspond to $\sqrt{3/2}$ and $\sqrt{3}/4$ of the lattice edge length of the matrix, respectively, and their ratio can be estimated to be equal to $\sqrt{2}$ exactly, so that it is reasonable to assign a cubic lattice for this phase. It is known from the preparation of specimens that the composition of this phase is not beyond the combination of the systems of CaO, SrO, Al_2O_3 and $CaSO_4$, although we do not know its exact composition. In the phases known in these systems, the extra spots can be indexed based on $Sr_3Al_2O_6$ with a lattice parameter of $a = 1.582$ nm proposed by Lagereqvist *et al.* [12]. The calculated plane spaces of $(2\,0\,0)$ and $(1\,1\,0)$ of the $Sr_3Al_2O_6$ phase are 0.791 and 1.119 nm, respectively, and they coincide with the measured values of 0.79 and 1.12 nm very well. Therefore the error of indexing based on lattice parameter is less than 0.6%. Consequently it is suitable to consider the inclusion as the $Sr_3Al_2O_6$ phase, a very complex oxide of the binary system of SrO and Al_2O_3 for 24 molecules contained in its unit cell. The extra spots along the $[1\,1\,\bar{1}]^*$ and $[1\,1\,2]^*$ directions correspond to the $(0\,0\,2)$ and $(1\,1\,0)$ planes, respectively, and thus Fig. 10 is an electron diffraction pattern composed of $(\bar{1}\,1\,0)^*$ reciprocal planes of the $2*d_{1\,1\,0}$ superstructure in the $[1\,1\,2]$ 180° rotation twin-related positions, and the $(1\,\bar{1}\,0)^*$ reciprocal plane of $Sr_3Al_2O_6$ phase. Moreover, the orientation relationship between them could also be deduced from this composited pattern as follows

$$(1\,1\,\bar{1})_m//(0\,0\,1)_p,\ (1\,1\,2)_m//(1\,1\,0)_p,\ [\bar{1}\,1\,0]_m//[1\,\bar{1}\,0]_p$$

where m and p express superstructures of $Ca_3SrAl_6SO_{16}$ and $Sr_3Al_2O_6$, respectively. The orientation relationship between the $Ca_3SrAl_6SO_{16}$ matrix and this binary phase can also be predicted to be the same as above if they co-exist. This oxide phase, formed at about 1200 °C or a somewhat higher temperature, may be an intermediate product during the path of the solid reaction in the preparation. Its existence seems to be closely related to its situation as an inclusion between the two twin variants of the superstructure,

which may prevent it from further phase transformation in the process of preparation.

4. Conclusions

The investigation of C_4A_3S and $Ca_3SrAl_6SO_{16}$ using the HREM technique reveals various interesting variations of their microstructures in local areas. The advantages of this method are that it can reveal structural irregularities in crystals in local areas directly, and the details of twin interface shown in the HREM image thus allow us to decide unambiguously on the type of twinning both in the cases of C_4A_3S and its superstructure. In combination with the image simulation, a possible structure model of [1 1 2] 180° rotation twinning was also proposed, and the non-stoichiometric interface may be introduced in this model. This may be the first report of twinning found in cement clinker with an ultramarine-like structure in the ternary system of CaO, Al_2O_3 and $CaSO_4$. The remainder of the other phase, possibly having cubic symmetry, with a lattice parameter very close to that of $Sr_3Al_2O_6$, was examined as an inclusion inside the twin-oriented superstructure of $Ca_3SrAl_6SO_{16}$, and the coherent interphase boundaries as well as the orientation relationship between them were discovered. The situation of the inclusion may be favourable to its existence in the cement clinker.

References

1. T. A. RAGOZINA, *Zh. Prikl. Khim.* **30** (1957) 1682.
2. P. E. HEALSTED and A. E. MOORE, *J. appl. Chem.* **12** (1962) 413.
3. X. J. FENG, G. L. LIAO and S. Z. LONG, *J. Chin. Silicate Soc.* **18** (1990) 310.
4. F. M. JAEGER, in "Georger Fisher Baher Memorial Lectures", Part III (Cornell University, 1930) 7.
5. G. L. LIAO, Dissertation, Wuhan University of Technology (1988).
6. Y. G. WANG, H. Q. YE, K. H. KUO, X. J. FENG, G. L. LIAO and S. Z. LONG, *J. Mater. Sci.*, **25** (1990) 5147.
7. K. ISHIZUKA, *Acta Cryst.* **A38** (1982) 773.
8. M. V. KLASSEN-NEKLYUDOVA, "Mechanical twinning of crystals" (McGraw-Hill, London, 1964) p. 65.
9. Y. G. WANG, H. Q. YE, K. H. KUO, X. J. FENG, G. L. LIAO and S. Z. LONG, *J. Mater. Sci.* **??** (1990) **xxx**.
10 W. BOLLMAN, "Crystal defects and crystalline interfaces" (Springer-Verlag, Berlin, 1970) p. 50.
11. Y. G. WANG, H. Q. YE, K. H. KUO, X. J. FENG, G. L. LIAO and S. Z. LONG, *J. Mater. Sci.* (1990). ?
12. E. A. LAGERQVIST *et al.*, *Z. Anorg. Allgem. Chem.* **234** (1937) 1.

Received 9 April 1990
and accepted 15 January 1991